RSC Advances

This is an *Accepted Manuscript*, which has been through the Royal Society of Chemistry peer review process and has been accepted for publication.

Accepted Manuscripts are published online shortly after acceptance, before technical editing, formatting and proof reading. Using this free service, authors can make their results available to the community, in citable form, before we publish the edited article. This *Accepted Manuscript* will be replaced by the edited, formatted and paginated article as soon as this is available.

You can find more information about *Accepted Manuscripts* in the **Information for Authors**.

ROYAL SOCIETY OF CHEMISTRY

www.rsc.org/advances

First-principles Calculations of Graphene-Based Polyaniline Nano-hybrids for Insight of Electromagnetic Properties and Electronic Structures

Yuping Duan, Jin Liu, Yahong Zhang, Tongmin Wang∗

Abstract

In situ polymerization between aniline and ammonium persulfate (APS) under acidic conditions is described for the preparation of graphene-based polyaniline hybrids with investigation of their electromagnetic properties. Samples were characterized by X-ray diffraction (XRD), Raman spectroscopy, Fourier transform infrared (FTIR), scanning electron microscopy (SEM), transition electron microscopy (TEM) and vector network analysis. The results revealed that the graphene-based PANI hybrids formed a uniform PANI particle coating on the graphene sheets. Such special structures lead to π-π interactions between graphene and PANI, and thus the electromagnetic absorption properties are significantly improved versus pure conducting polymers. The maximum reflection loss reaches -32.1dB at 5.45 GHz with a thickness of 4 mm. The bandwidth (RL<-10 dB) reaches an amazing 5.62 GHz with a thickness of 2 mm. In particular, first-principles calculations based on density function theory (DFT) were carried out to uncover the relationship between dielectric properties and electronic structures.

Key Laboratory of Solidification Control and Digital Preparation Technology (Liaoning Province), School of Materials Science and Engineering, Dalian University of Technology, Dalian 116085, P.R. China
∗ Corresponding author. Tel: +86 411 84708446; fax: +86 411 84708446
E-mail address: tmwang@dlut.edu.cn; duanyp@dlut.edu.cn;

Key words: Graphene, Polyaniline, Microwave dielectric, First-principles

1. Introduction

In recent years, the interactions between materials and microwaves have drawn wide attention due to the rapid development of electronic devices ranging from civil to military fields.[1-4] Devices using lower frequency range microwave radiation such as mobile phones, LAN systems, and radar are especially exciting. Meanwhile, associated serious electromagnetic interference (EMI) and military defense problems are becoming apparent. Electromagnetic shielding is an effective way to restrain electromagnetic radiation, but this method cannot fundamentally remove the threat of radiation.[5-6]

Electromagnetic wave absorbing materials are a practical method to consume electromagnetic waves.[7-9] There is a greater demand for lightweight, flexible, wide-band absorbing materials in applications where attenuation is the primary necessity.[10] Therefore, the recombination of material has resulted in remarkable success to improve materials properties. Much attention has been given to the study of microwave-absorbent materials.

Of the various types of absorbents, graphene—a one-atom-thick planar sheet of sp2-bonded carbon atoms that are densely packed in a honeycomb crystal lattice—has attracted much attention because of its remarkable properties.[11] Since the first report of graphene as a microwave absorbent, the synthesis and doping of graphene absorbent composites have been explored extensively. Sun et al.[12] reported a facile solvothermal route to synthesize laminated magnetic graphene, and subsequent

research suggested that there are significant changes in the electromagnetic properties of magnetic graphene versus pure graphene. The results show that reflection loss below -10dB was obtained at 10.4-13.2GHz, which confirms that graphene is a highly desirable electromagnetic wave absorber.

Wang and co-workers[13] prepared chemically reduced graphene oxide by a modified Hummers method and discussed the microwave absorption properties. The results indicate that r-GO exhibits much better microwave absorbing ability than graphite. Polyaniline (PANI) is one of the most promising conducting polymers, has excellent environment stability and high electrical conductivity, and can absorb microwaves.[14-16] The emeraldine base (EB) form of PANI is neutral, whereas the emeraldine salt (ES) form (protonated at imine nitrogen atoms) has good conductivity. This is because protonation helps delocalize the otherwise trapped diiminoquinone-diaminobenzene state.[17] HCl is the most common doping agent used to achieve ES form during PANI polymerization, and polyaniline films have been used as effective absorbers of electromagnetic radiation,[18, 19] but the absorption values are far below other doped absorbents.

To improve the absorbing properties of the PANI, research has been focused on studies of doping the PANI composites.[20, 21] The electrical conductivity and electromagnetic response can be properly improved by incorporating conductive fibers such as carbon nanotubes and graphene. Yu et al.[22] reported a *situ* polymerization progress to synthesize graphene/polyaniline nanorod arrays, and the maximum reflection loss is -45.1 dB with a thickness of 2.5 mm. Reduced graphene

oxide with polyaniline film composites (2 mm film) exhibit high reflection loss values approaching -41.4 dB at 13.8 GHz, which may be attributed to the unique structural characteristics and charge transfer between RGO and PANI film.[23]

In another study, Qiu et al.[24] developed PANI-based multi-walled carbon nanotube nanocomposites. They demonstrated that there were strong interactions between the π-bonded surface of the MWCNTs and quinoid rings of PANI, which contributed to the microwave-absorbing properties. While many researchers have focused on the microwave absorption properties of PANI, there are relatively few reports on the microwave properties of PANI films on the surface of graphene. Here, we show such performance and offer a theoretical explanation based on first-principles calculation for the first time.

We investigated the microwave dielectric response and the correlative electromagnetic properties of graphene-based PANI composites. We show how these features are influenced by the doping ratios of the two elements. The synthesis and analysis of graphene-based PANI composites are carried out with *in situ* polymerization. To study the dielectric response comprehensively, the analyses are mainly divided into two parts: on the macroscopic scale, the dielectric response and its derived properties are discussed; on the microscopic scale, the theoretical explanation based on fist-principles calculations are included. To the best of our knowledge, this is one of the first articles to systematically describe the microwave dielectric response of graphene-based PANI.

2. Experimental procedure

2.1 Synthesis

All chemicals were of analytical grade and used without further purification. The facile synthesis of graphene-based polyaniline hybrids by *in situ* polymerization was conducted in aqueous solution with ammonium persulfate (APS) as an oxidant as described elsewhere with minor modifications.[25] First, different amounts of graphene were added to 25 mL 1 N HCl aqueous solution under ultrasonication for 30 min. Subsequently, 2.5 mL of aniline was dissolved in 25 mL 1 N HCl solution and then transferred to the above solution under stirring for 1 h. After that, 27.2 mmol of APS dissolved in 25 mL 1 N HCl aqueous solution was slowly added to the above-mentioned mixture, and the resulting solution was mechanically stirred for about 1 h. The mixture was maintained for polymerization for 24 h. When the reaction was finished, the dark green product was rinsed with deionized water and ethanol for three times to remove the undesired content. Finally, the precipitate was dried at 60°C for 24 h. The mass ratios of graphene to aniline in the starting solutions were increased gradually from 0 to 13 percent. These samples were denoted as S1, S3, S3, S4 and S5 corresponding to different mass proportions of graphene (0, 4, 7, 10 and 13, respectively).

2.2 Characterization

The morphologies and sizes of the synthesized products were observed on a field emission scanning electron microscope (SEM, SUPRA55) and a transition electron microscope (TEM, Tecnai G220 S-Twin). The crystal structures of the materials were determined by X-ray diffraction (XRD, Empyrean) analyses with Cu Kα radiation,

using an operating voltage and current of 40.0 kV and 40.0 mA, respectively. The

scanning range was from 10.00° to 80.00° (2θ), and the scan speed was 2.00°/min.

Raman spectra were recorded on a Laser Raman spectroscopy (Invia, RENISHAW)

using a 514 nm argon ion laser. Fourier transform infrared (FTIR) spectra were

observed by a Bruker Vertex-70 FTIR spectrometer from 4000 to 400 cm^{-1}.

2.3 Electromagnetic Measurement

The relative complex permittivity and permeability versus frequency were

carried out by coaxial reflection/transmission method using an Aglient 8722ES vector

network analyzer with a working frequency at 2-18 GHz. The measured products

were prepared by uniformly mixing 20 wt% of the sample with a paraffin matrix. The

obtained mixtures were molded into toroidal-shaped samples of 7.00 mm outer

diameter and 3.00 mm inner diameter. Transmission line theory was introduced to

compute the wave-absorbing properties, which is appointed as reflection loss (RL).

2.4 Simulation method

The first-principles quantum mechanical calculations based on density functional

theory (DFT) were performed with the approximation of Perdew, Burke, and

Ernzerhof (PBE) utilizing the generalized gradient approximation (GGA) scheme

provided by the CASTEP module.

3. Results and discussion

3.1 Structure analysis

Figure. 1 shows the XRD patterns of the graphene, PANI and graphene-based

PANI nanocomposite (S3). Graphene exhibits two diffraction peaks at 2θ=26.4° and

43.2° that can be attributed to the graphite-like structures (002) and (100), respectively. The broad nature of diffraction peaks illustrates poor crystallinity along the graphene sheet stacking direction. This confirms that the samples consist of a few layers of graphene sheets that are different from crystalline graphite. For PANI, the semicrystalline peaks appear at 2θ=15.1°, 20.6° and 25.6°. These correspond to the (011), (020) and (200) crystal planes of PANI in its emeraldine salt (ES) form, respectively.[26]

In the graphene-based PANI composite, the XRD pattern presents three peaks similar to PANI confirming that no additional crystal structure has been introduced into the composite. However, the diffraction peak at 43.2° of graphene disappears indicating that graphene is fully interacted with PANI molecules and completely covered by PANI particles. It should be noted that the patterns of S1, S2, S4 and S5 are nearly identical to S3. Preliminary analysis suggests that the content of PANI is sufficient to coat the graphene sheets.

Figure. 2 shows typical FTIR spectra of graphene, PANI, and graphene-based PANI nanocomposites prepared with different doping contents. For graphene, the broad band at 1575 cm^{-1} could be ascribed to the C=C stretching sp^2 hybridized carbon atoms of graphene. For pure PANI, the characteristic bands at 1558 and 1479 cm^{-1} are assigned to the C=C stretching of quinoid and benzenoid rings, respectively. Meanwhile, the bands at 1304 cm^{-1}, 1243 cm^{-1} and 1123 cm^{-1} are due to the C-N stretching of the secondary aromatic amine and C-H bending of the benzenoid and quinoid rings, respectively.[27] The spectra of graphene-based PANI composites exhibit

similar vibrational bands as pure PANI suggesting that graphene has been successfully covered by PANI. However, a slight shifting and broadening of the characteristic bands were also observed with increasing graphene ratios. This indicates the existence of interactions between graphene and PANI. Versus pure PANI, the characteristic peaks due to C-N stretching are shifted slightly to 1301 and 1299 cm^{-1}, which might be ascribed to the π-π interactions between the PANI molecules and graphene.

The formation of graphene, PANI, and graphene-based PANI hybrids were confirmed with Raman scattering as shown in Figure. 3. The Raman spectrum of graphene displays three dominant peaks at 1345, 1573 and 2683 cm^{-1} known as the D, G, and 2D bands, respectively.[28] The D band is associated with disordered carbon materials, while the G band is the result of the first-order scattering of the E_{2g} mode of sp^2 carbon domains.[29] Both bands can be influenced by doping. For the pure PANI in Figure. 3, the bands at 1166 and 1490 cm^{-1} were associated with C-H bending deformation in the benzenoid ring and C=N stretching band of quinoid rings, respectively. It is noteworthy that the vibrations of the semiquinone radical and C=C stretching of quinoid rings of PANI at 1332 and 1591 cm^{-1}, respectively, have merged with the D band and G band of graphene. This shows the strong interaction between PANI and graphene in the graphene-based PANI hybrid. On the one hand, the intensity of the C-H bond at 1166 cm^{-1} and C=N stretching at 1490 cm^{-1} increase remarkably. On the other hand, these four peaks of PANI exhibit redshifts to different degrees. Overall, for the graphene-based PANI hybrids, a π-π interaction between the quinoid ring of PANI and the π-electrons in graphene existed. The interaction is

believed to facilitate charge transfer between graphene and PANI. This influences the

absorbing properties.

3.2 Microstructure and morphologies

The SEM and TEM images in Figure. 4 illustrate the morphology and texture of

the pure PANI, graphene, and graphene-based PANI hybrids. As shown in Figure. 4

(a), PANI particles form worm-like agglomerates 200 nm in diameter and 500 nm

long. From Figure. 4 (b) shows multi-layered graphene sheets with layer numbers of

4-6 that are easily distinguished from the folded edge. As a support material,

multi-layered graphene could supply large numbers of active sites for nucleation of

PANI, and PANI nanofibers are well distributed on the graphene sheets (Figure. 4 (d)).

However, the morphology of the resulting PANI nanofibers is affected by the

graphene sheets in the polymerization as apparent from the SEM images shown in

Figure. 4 (c). Many uniform PANI nanoparticles intertwine each other and embed

compactly in the graphene. The average diameter of the PANI nanoparticles is 100 nm.

The analysis above demonstrated that graphene sheets are completely and

successfully covered by nanostructured PANI. This may be favorable for the

enhancement of charge transfer between graphene and PANI and conductive to the

dielectric properties of composites.

Based on these results, we propose a formation mechanism of graphene-based

PANI hybrids and a charge-transfer complex between graphene and PANI as a

consistent explanation of all of the aforementioned experimental observations as

depicted in Figure. 5. After adding aniline to the mixed suspension of HCl and

graphene, aniline monomers can immediately adsorb on the surface of graphene as a result of the electrostatic attraction. An *in situ* polymerization occurred when the oxidant APS were added. Thus, a large amount of PANI nuclei is generated on the graphene surface at the beginning of the polymerization process by heterogeneous nucleation. Afterward, the initial nuclei grew to form nanoparticles at the adsorbing sites of graphene surface. Upon polymerization without graphene, the PANI particles form worm-like agglomerates. Here, the graphene is a good electron acceptor and aniline is a good donor. There is an equilibrium between both species through charge transfer along the interface of graphene and PANI.

3.3 Electromagnetic Properties

For an electromagnetic wave absorber, relative complex permittivity ($\varepsilon_r = \varepsilon' - \varepsilon''$) and permeability ($\mu_r = \mu' - \mu''$) play an important role in determining the absorption properties. The real parts of the relative complex permittivity and permeability symbolize the energy storage, and the imaginary parts represent energy loss. The energy storage describes the lossless portion of the exchange of energy between the field and the material, and energy dissipation occurs when electromagnetic energy is absorbed by the material.[30] Here, the relative complex permittivity and permeability of the composites were studied and typical parameters in the range of 2-18 GHz for five samples composed of S0, S1, S2, S3, S4 and S5 are shown in Figure. 6, respectively.

From the Figure. 6 (a), it is clear that the real parts ε' of the five sample decrease gradually with increasing frequency. This is dielectric dispersion. The real

parts ε' of S3 and S4 show more distinct response characteristic than the other samples. PANI is a dielectric loss material, and its permittivity is tightly related to the Debye dipolar relaxation process at microwave frequency ranges. When an electromagnetic field is applied, the random dipoles of the composite will change their orientation to be parallel to the external field leading to dipole relaxation polarization.

In practice, however, there is much resistance to overcoming the energy loss process. As the electromagnetic frequency increased to a critical point, the re-arrangement of the dipoles cannot keep pace with the fast-changing external electromagnetic field and makes almost no contribution to the dielectric polarization.[31] Thus, the dielectric response tends to gradually decrease with increasing frequency as shown in Figure. 6 (a). When the reactions are carried out with graphene (S3, S4, and S5), the ε'' values are larger than those of pure PANI due to their strong attenuation potential, which can result in excellent dielectric loss properties.

Figure. 6 (b) shows the relative complex permeability variation of a series of samples in the 2-18 GHz range. The real parts (μ') increase as the graphene is introduced. Despite this, both the real parts (μ') and the imaginary parts (μ'') of the relative complex permeability remain relatively stable around 1.00 and 0.00 in the whole frequency range. This demonstrates that the graphene-based PANI composites exhibit weak magnetic characteristics and reflection loss is mainly attributed to electrical loss. This is decided by dipole relaxation polarization process.

To directly describe the dielectric loss, we have also calculated the dielectric loss tangent (tan$\delta_E = \varepsilon''/\varepsilon'$) based on the permittivity of samples measured above (Figure. 7). The dielectric loss tangent of all the five samples increase with increasing frequency, and the values of S3 and S4 are higher than those of other samples within the entire frequency range. We concluded that the dielectric loss of PANI is dramatically improved by doping with graphene—especially when the ratio of graphene is 7 wt% and 10 wt%. Nevertheless, the magnetic loss tangent (tan$\delta_\mu = \mu''/\mu'$) in the range of 2-18 GHz is less than 0.1 (not shown) suggesting a negligible contribution from magnetic loss. This result corresponds to the analysis of electromagnetic parameters.

3.4 Conductivity properties

In addition to the complex permittivity and permeability, dielectric conductivity is another important parameter determining the dielectric response. According to the free-electron theory, dielectric conductivity can be given as:[31]

$$\sigma = \omega \varepsilon_0 \varepsilon'' \tag{1}$$

where ω is angular frequency ($\omega = 2\pi f$), and ε_0 and ε'' are the dielectric permittivity of the free space and imaginary part of relative permittivity. The curves of dielectric conductivity based on Equation. (1) are shown in Figure. 8. The dielectric conductivity grows with increasing frequency, but the low concentration of graphene (4wt%) makes unconventionally decreases the conductivity versus pure PANI. This was mainly caused by the hybridizing interactions between PANI and graphene. The interaction resulted in more defects and disordered parts that destroyed the large

12

conjugated system in graphene. However, with increasing graphene content, the values of conductivity become larger due to the high conductivity of graphene. As a result, the concentrations of the charge carriers can be adjusted by introducing different proportions of graphene.

3.5 First principles study of electronic structure

We also used first-principle calculations based on density functional theory (DFT) to study the relationship between the dielectric properties and electronic structures. The calculations were performed using the CASTEP module of Accelrys' material studio.[32] The structure optimization and corresponding energy calculations were based on the generalized gradient approximation (GGA) function with the Perdew-Burke-Ernzerhof (PBE) correction.[33] The k-point was set to 4×4×1 for all slabs with a cutoff energy of 400 eV. A Gaussian smearing of 0.1 eV was used for Fermi surface broadening. In addition, molecular dynamic simulations were carried out to investigate the microscopic mechanism of interactions on graphene-based PANI nanocomposites interface. The entire calculation process was carried out in reciprocal space.

The geometric structures and atomic arrangements contain 32 atoms in 4×4 intrinsic graphene. These adsorb a segment of polyaniline and are summarized in Figure. 9. Meanwhile, Figure. 9 shows the interaction configurations of graphene-based PANI system at different simulation times at 300 K. The figure shows that the PANI molecule moves close to the graphene sheet as a function of time. After 30 ps, the distance between graphene sheet and PANI molecule is 3.4 Å. During this

interaction, the benzene ring tends to be parallel to the graphene surface indicating that there was a strong attraction of graphene for PANI. The strong interaction gradually pulled PANI toward the graphene and avoided leaving the surface of graphene. The graphene-based PANI system reached equilibrium in a relatively short period of time. This was a thermodynamic equilibrium system.

The formation energy of optimized structures is defined as:

$$E_{interaction} = E_{total} - \left(E_{PANI} + E_{graphene}\right) \qquad (2)$$

where E_{total}, E_{PANI} and $E_{graphene}$ denote the total energies of the complex, a segment of PANI and the intrinsic graphene, respectively. The calculated $E_{interaction}$ is a measure of the strength of the interaction between two interacting molecules.

Equation. (2) shows that a binding energy of -16.6 kcal/mol was obtained. The negative value meant that the PANI molecules can be thermodynamically adsorbed on graphene. The adsorbed polyaniline molecule was found floating above the graphene sheet at 3.4 Å with no evidence of a chemical bond between them. A charge transferred of 0.02 e from the PANI molecule to the graphene was found. To better understand the influence of special adsorbed structure on dielectric properties, the electronic density of states (DOS) were also obtained (Figure. 10).

The intrinsic graphene was a zero-gap semiconductor and its Fermi energy exactly crossed the Dirac point, which agreed with the calculated results of other research.[34] The electronic energy spectra suggest strong hybridization between PANI molecule and carbon atoms of graphene at 3.5, -1.8, -3.5, -6.3, -8.9, -14, -16.5 and -19.5 eV. The outermost orbital configurations of the excited C atoms in graphene are

$2s^1 2p^3$, and the electron transferred from the PANI molecule changes the original filling condition of 2p orbitals. Thus, the dipole polarization intensity is enhanced at the applied field. Meanwhile, the displacement of the outer electron clouds might lead to electronic polarization. We predict that the dielectric properties will be improved based on the theoretical analysis and this prediction agrees well with our experimental results.

3.6 Microwave absorbing properties

To further reveal the enhanced electromagnetic wave absorption properties of graphene-based PANI composites from 2-18 GHz, reflection loss (RL) was evaluated for various thicknesses of the absorbent (Figure. 11), according to the transmission-line theory.[35] The normalized input impedance Z_{in} can be expressed in the following form:

$$Z_{in} = \sqrt{\frac{\mu_r}{\varepsilon_r}} \tanh\left[j \frac{2\pi}{c} \sqrt{\mu_r \mu_r} f d\right] \qquad (3)$$

Where, μ_r and ε_r represent the relative permeability and permittivity of the composite, respectively; c is the velocity of electromagnetic waves in free space, f is the frequency of the microwave, and d is the thickness of the absorber. The relationship between the reflection loss and Z_{in} is expressed as

$$RL = 20 \left|\frac{Z_{in}-Z_0}{Z_{in}+Z_0}\right| \qquad (4)$$

Where $Z_0 = \sqrt{\mu_0/\varepsilon_0}$ is the characteristic impedance of free space, and Z_{in} is the input impedance of absorber. The minimum RL is equivalent to the occurrence of the minimum reflection of the incident microwave; in other words, the ratio of absorption reaches a maximum.[36] As shown in Figure. 11, with increasing absorber thickness, the

minimum RL for graphene-based PANI composites declines quickly, and the effective

bandwidth of each sample decreases. In addition, all of the RL peaks of the five

samples move toward lower frequency with increasing thickness.

In considering both the thickness and bandwidth (RL<-10 dB), sample S3 offers

better microwave absorption performance than other samples. Figure. 11(c) shows

that the maximum reflection loss reaches -32.1dB at 5.45 GHz for the PANI/graphene

(S3) with a thickness of 4 mm. The bandwidth is 1.8 GHz and is located at 4.7-6.5

GHz. It is -22.1 dB at 5.9 GHz for the PANI particles with the same thickness. When

the thickness is 2 mm, the bandwidth of S3 reaches an amazing 5.62 GHz, which is

located at 10.19-15.91 GHz and is much higher than the other samples. The

improvement of microwave absorption is attributed to two key factors: impedance

matching and electromagnetic wave attenuation.

According to (3) and (4), Z_0 should be equal to Z_{in} to realize the zero reflection

when the microwave is incident on the absorber. Thus, the relative complex

permittivity and permeability should satisfy the relationships of $\mu_r = \varepsilon_r$ or

$\tan\delta_\mu = \tan\delta_E$ for an ideal microwave absorbing materials. Thus, sample S3 with lower

$\tan\delta_E$ values than S4 (as shown in Figure. 7) exhibits a better impedance match. This

results in a stronger microwave absorption. Based on this theory, the values of $\tan\delta_E$

for sample S1 are closest to $\tan\delta_\mu$. However, the corresponding maximum RL is only

-12 dB with a thickness of 3 mm that was much lower than other samples. This is

because better impedance matching only means that a smaller part of the

electromagnetic wave is reflected in the air/absorber interface.

Electromagnetic wave attenuation is another important factor that contributes to microwave absorption. If the value of the loss tangent is too small, then it will also become a restricted condition for effective attenuation of the incident microwave. It is also believed that the special hybridizing structure of graphene and PANI would generate many defects and act as polarization centers to cause polarization relaxation under altered electromagnetic fields. This leads to energy dissipation.

Therefore, both impedance matching and microwave attenuation should be considered simultaneously to obtain excellent absorbance. This analysis demonstrates that the as-synthesized graphene-based PANI composite offers better microwave absorption performance via doping with the appropriate graphene ratios and adjusting the thickness.

5. Conclusion

In summary, different proportions of graphene-based PANI composites were synthesized using in situ polymerization. The hybrid material with uniform PANI nanoparticles coated on the graphene sheets was obtained. Special π-π interactions between graphene and PANI exist, and thus the electromagnetic properties are significantly improved versus pure conducting polymers. First-principle calculations show significant hybridization and charge transfer between PANI and graphene sheets. This gives rise to the enhanced dipole polarization intensity.

At 7% graphene, the graphene-based PANI composites had the best microwave-absorbing properties: the maximum reflection loss reaches -32.1dB at 5.45 GHz with a thickness of 4 mm, and the bandwidth (RL<-10 dB) reaches and

amazing 5.62 GHz with a thickness of 2 mm. This improvement in microwave absorption is attributed to two key factors: impedance matching and electromagnetic wave attenuation. Thus, the deposition of PANI molecules on the surface of graphene sheets is an efficient way to prepare absorbents with strong dielectric attenuation.

Acknowledgements

References

1 W. M. Zhu, L. Wang, R. Zhao, J. W. Ren, G. Z. Lu, Y. Q. Wang, *Nanoscale*, 2011, *3*, 2862.

2 H. B. Zhang, Q. Yan, W. G. Zheng, Z. He, Z. Z. Yu, *ACS Appl. Mat. Interfaces*, 2011, 3, 918.

3 Z. P. Wu, M. M. Li, Y. Y. Hu, Y. S. Li, Z. X. Wang, Y. H. Yin, Y. C. Chen, X. Zhou, *Scripta Mater*, 2011, 64, 809.

4 H. Yang, M. Cao, Y. Li, H. Shi, Z. Hou, X. Fang, H. Jin, W. Wang, J. Yuan, Adv. Opt. Mater., 2014, 2, 214.

5 Y. Huang, N. Li, Y. Ma, F. Du, F. Li, X. He, X. Lin, H. Gao, Y. Chen, *Carbon*, 2007, 45,1614.

6 M. C. Gupta, Y. Yang, K. L. Dudley, R. W. Lawrence, *US patent*, 2013,8424200.

7 Y. Qing, W. Zhou, S. Jia, F. Luo, D. Zhu, J. *Mater. Sci.*, 2010, 45, 1885.

8 X. Ding, Y. Huang, S. Li, J. Wang, *RSC Adv.*, 2016, 6. 31440.

9 R. Zhang, X. Huang, B. Zhong, L. Xia, G. Wen, Yu Zhou, *RSC Adv*, 2016, 6, 16952.

10 C. M. Watts, X. Liu, W. J. Padilla, Adv. Mater., 2012, 24.

11 K. S. Novoselov, *Nat. Mater.*, 2007, 6,183.

12 X. Sun, J. He, G. Li, J. Tang, T. Wang, Y. Guo, H. Xue, *J. Mater. Chem. C*, 2012, 1, 765.

13 C. Wang, X. Han, P. Xu, X. Zhang, Y. Du, S. Hu, J. Wang, X. Wang, *Appl. Phys. Lett.*, 2011, 98, 975.

14 M. M. M. Ahmed, T. Imae, *Phys. Chem. Chem. Phys.*, 2016, 18, 10400.

15 S. Yu, F. Qin, G. Wang , *J. Mater. Chem. C*, 2016, 4, 1504.

16 Q. Hao, X. Xia, W. Lei, W. Wang, J. Qiu, *Carbon*, 2015, 81, 552.

17 A. G. MacDiarmid, *Angew. Chem. Int. Ed.*, 2001, 40, 269.

18 T. Mäkelä, J. Sten, A. Hujanen, H. Isotalo, *Synth. Met.*, 1999, 101, 707.

19 T. Mäkelä, S. Pienimaa , T. Taka, S. Jussila, H. Isotalo, *Synth. Met.*, 1997, 85, 1335.

20 J. Joo, C. Y. Lee, *J. Appl. Phys.*, 2000, 88, 513.

21 Pa. Saini, V. Choudhary, K. N. Sood, S. K. Dhawan, *J. Appl. Polym. Sci.*, 2009, 113, 3146.

22 H. Yu, T. Wang, B. Wen, M. Lu, Z. Xu, C. Zhu, Y. Chen, X. Xue, C. Sun, M. Cao, *J.mater.chem.*, 2012, 22, 21679.

23 P. Liu, Y. Huang, *J. Polym. Res.*, 2014, 21, 1.

24 H. Qiu, J. Wang, S. Qi, Z. He, X. Fan, Y. Dong, *J. Mater. Sci. Mater. Electron*, 2014, 26, 564.

25 X. Chen, F. Meng, Z. Zhou, X. Tian, L. Shan, S. Zhu, X. Xu, J. Man, W. Li, D. Hui,

Y. Wang, J. Lu, J. Gou, *Nanoscale*, 2014, 6, 8140.

26 H. K. Chaudhari, D. S Kelkar, *Polym. Int.*, 1997, 42, 380.

27 T. Remyamol, H. John, P. Gopinath, *Carbon*, 2013, 59, 308.

28 Z. Wang, N. Li, Z. Shi, Z. Gu , *Nanotechnology*, 2010, 21, 175602.

29 F. Tuinstra, J. L Koenig, *J.Chen.Phys.*, 1970, 53, 1126.

30 L. F. Chen, C. K. Ong, C. P. Neo, V. V. Varadan, V. K. Varadan, *John Wiley and

Sons*, 2004.

31 Y. Duan, Z. Liu, H. Jing, Y. Zhang, S. Li, *J. Phys. Chem.*, 2012, 22, 18291.

32 M. D. Segall, P. J. D. Lindan, M. J. Probert, C. J. Pickard, P. J. Hasnip, S. J. Clark,

M. C. Payne, *J. Phys. Condens. Mat.*, 2002, 14, 2717.

33 J. P. Perdew, K. Burke, M. Ernzerhof, *Phys. Rev. Lett.*, 1996, 77, 3865.

34 B. Seger, P. V. Kamat, *J. Phys. Chem. C*, 2009, 113, 799.

35 Y. Naito, K. Suetake, *Ieee.T, Microw. Theory.*, 1971, 19, 65.

36 Y. Duan, J. Chen, Y. Zhang, M. Wen, T. Wang, *J. Supercond. Nov. Magn.*, 2014, 27,

2139.

Captions for Figures

Figure.1 The XRD patterns of graphene, PANI and graphene-based PANI hybrids

(S3).

Figure. 2 FT-IR spectra of graphene, PANI, and graphene-based PANI

nanocomposites.

Figure. 3 Raman spectrum of graphene, PANI, and graphene-based PANI nanocomposites (S3).

Figure. 4 SEM image of pure PANI (inset exhibits TEM image of pure PANI) (a); TEM of graphene (b); SEM (c); and TEM (d) of graphene-based PANI composite.

Figure. 5 Schematic illustration of the formation of graphene-based PANI hybrids and charge transformation equilibrium between graphene and PANI.

Figure. 6 The microwave dielectric response of the composites: (a) relative complex permittivity (b) permeability of the composites.

Figure. 7 Dielectric loss tangent ($\tan\delta_E = \varepsilon''/\varepsilon'$) of PANI and PANI/graphene composites.

Figure. 8 Dielectric conductivity of PANI and graphene-based PANI composites.

Figure. 9 Interaction configurations of graphene-based PANI system at different simulation times.

Figure. 10 The electronic density of state (DOS) for intrinsic graphene and graphene-based PANI adsorbed system as well as the partial density of state (PDOS) for PANI and graphene. A dotted line indicates the Fermi level.

Figure. 11 The reflection loss of PANI and PANI/graphene composite samples with different content of graphene are shown in the frequency range of 2-18 GHz.
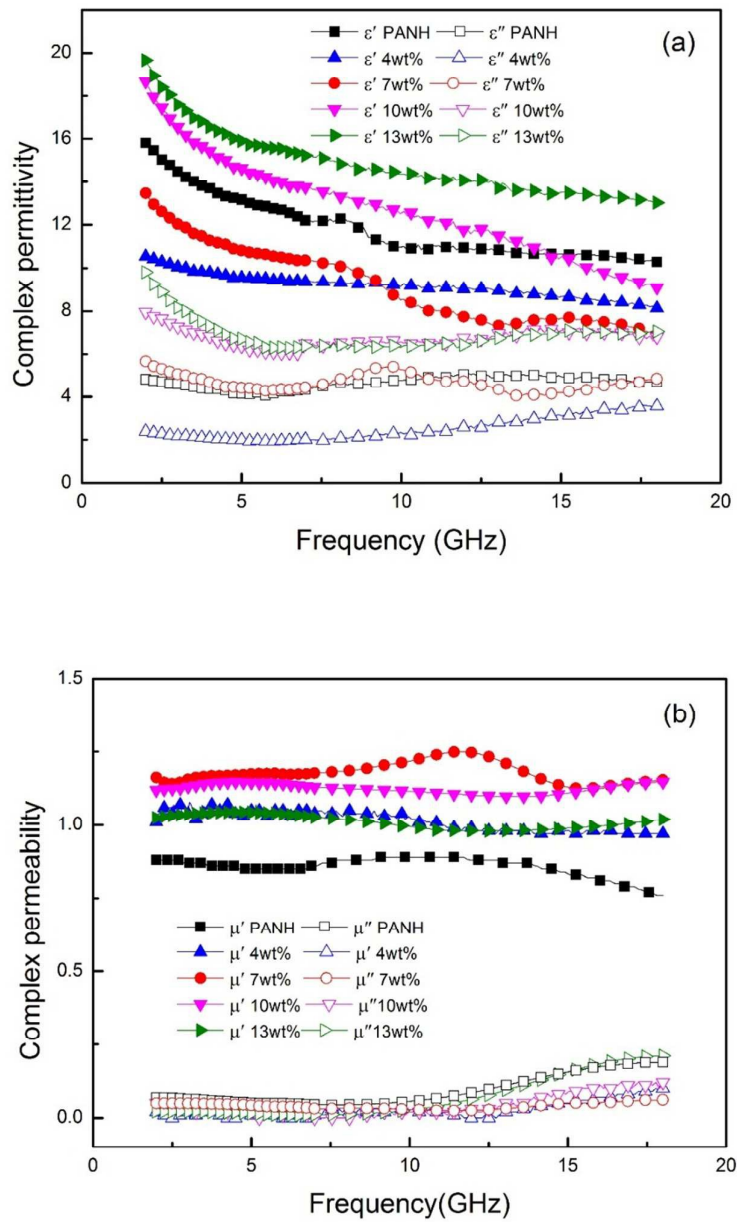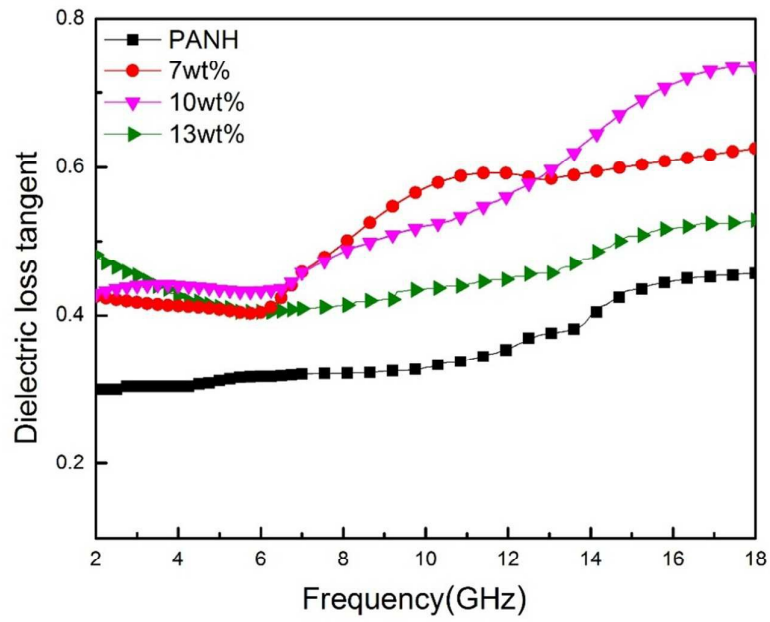
Figure 1
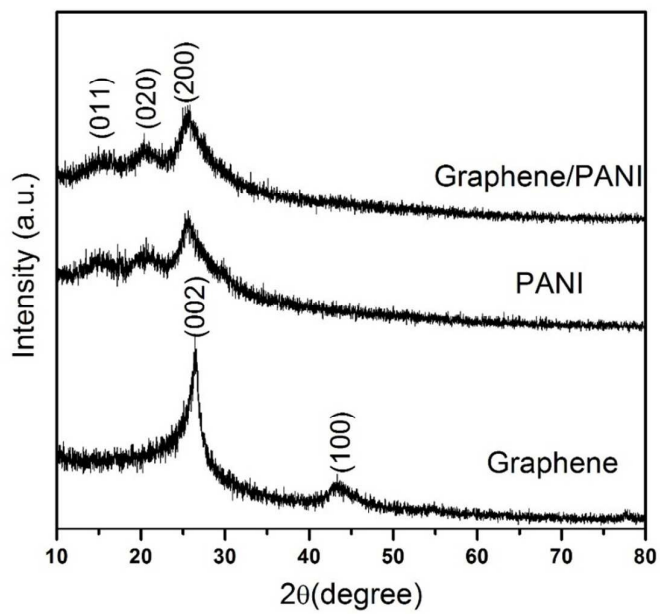
Figure 2
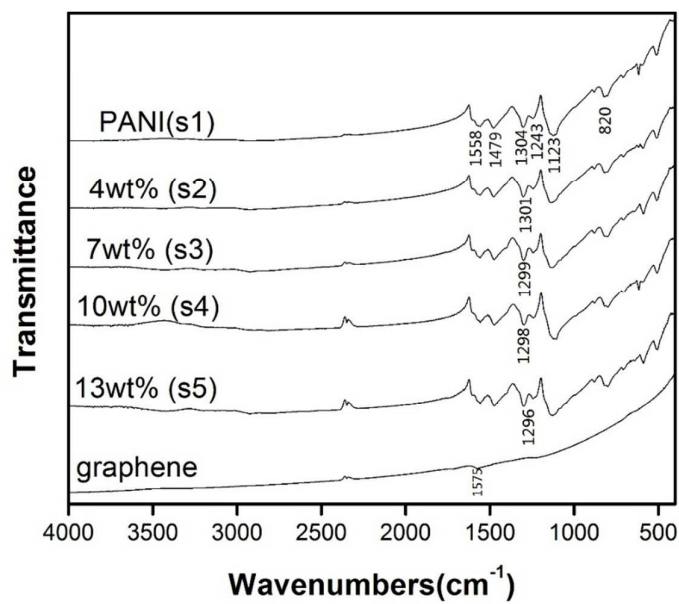
Figure 3
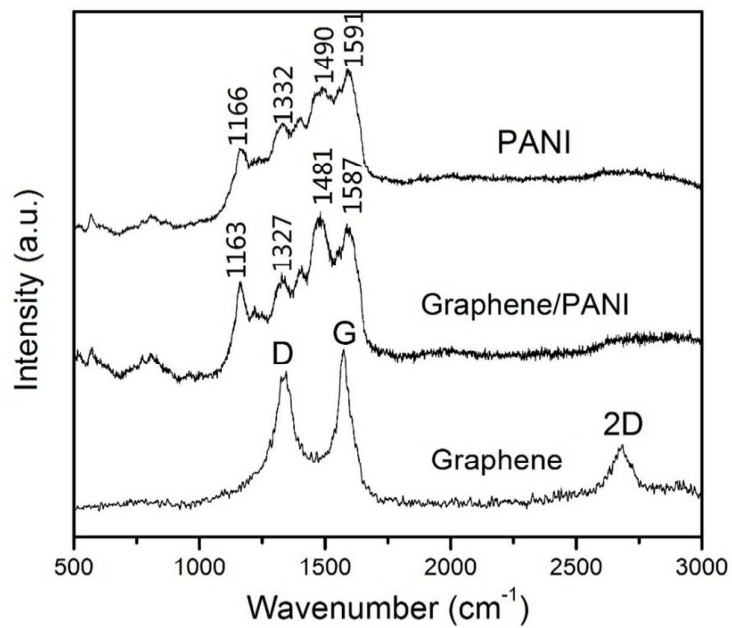
Figure 4
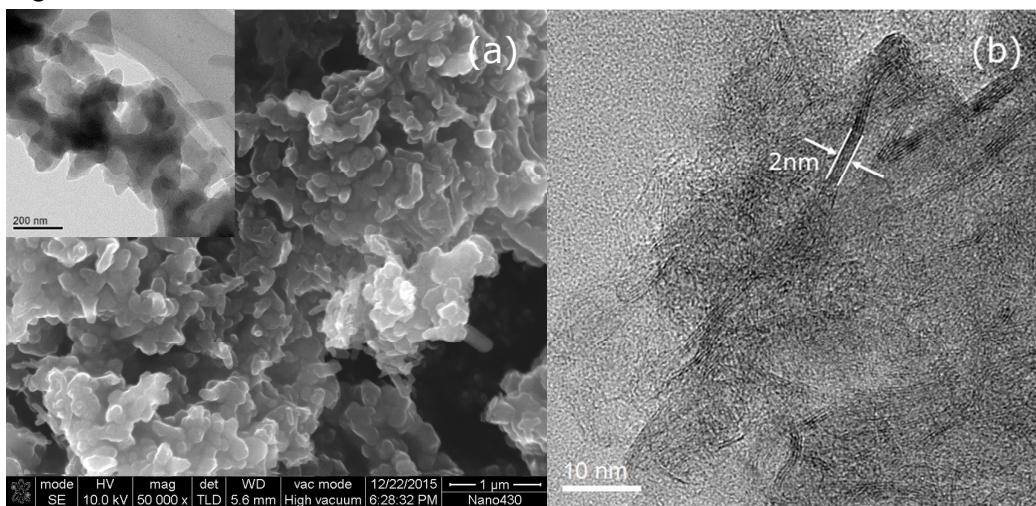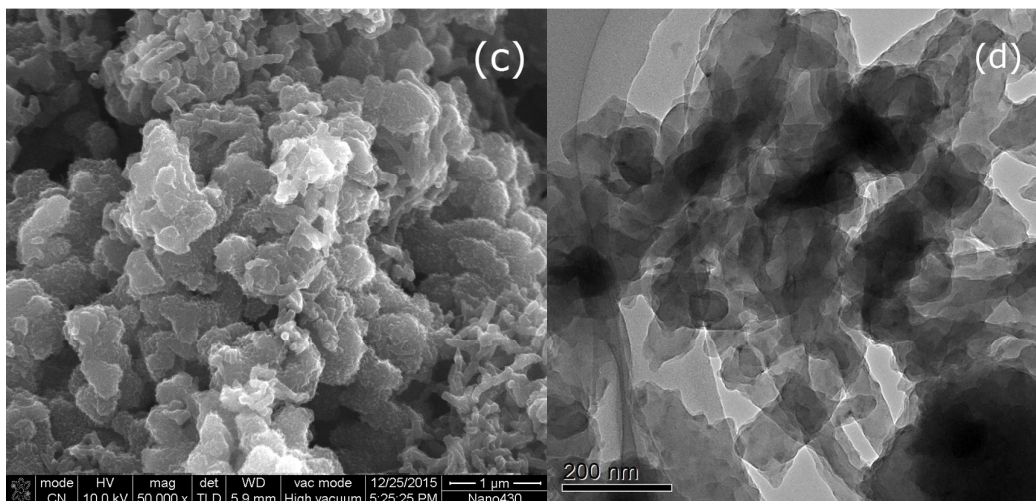
Figure 5
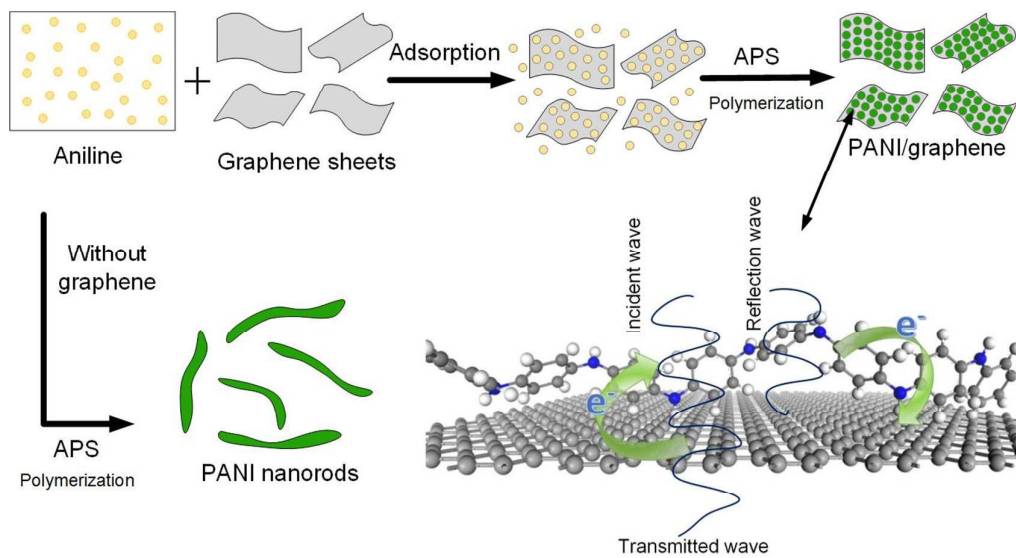
Figure 6

Figure 7

Figure8
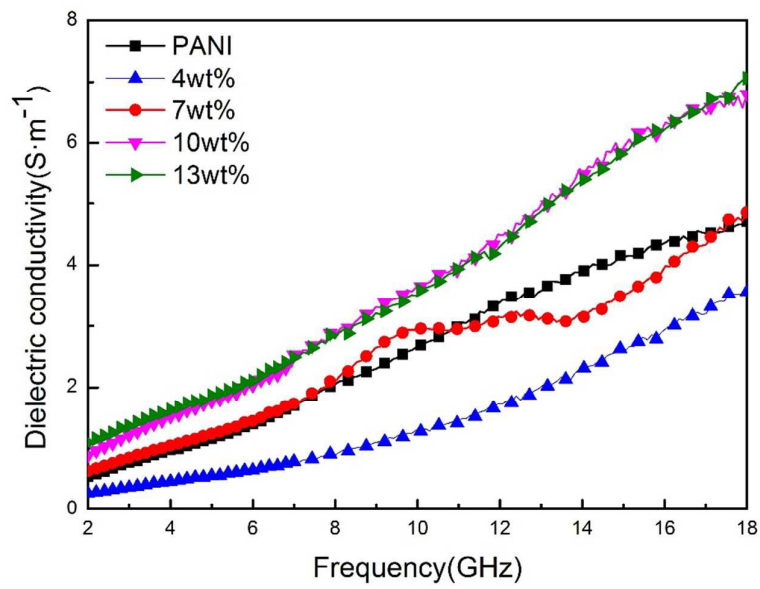
Figure 9
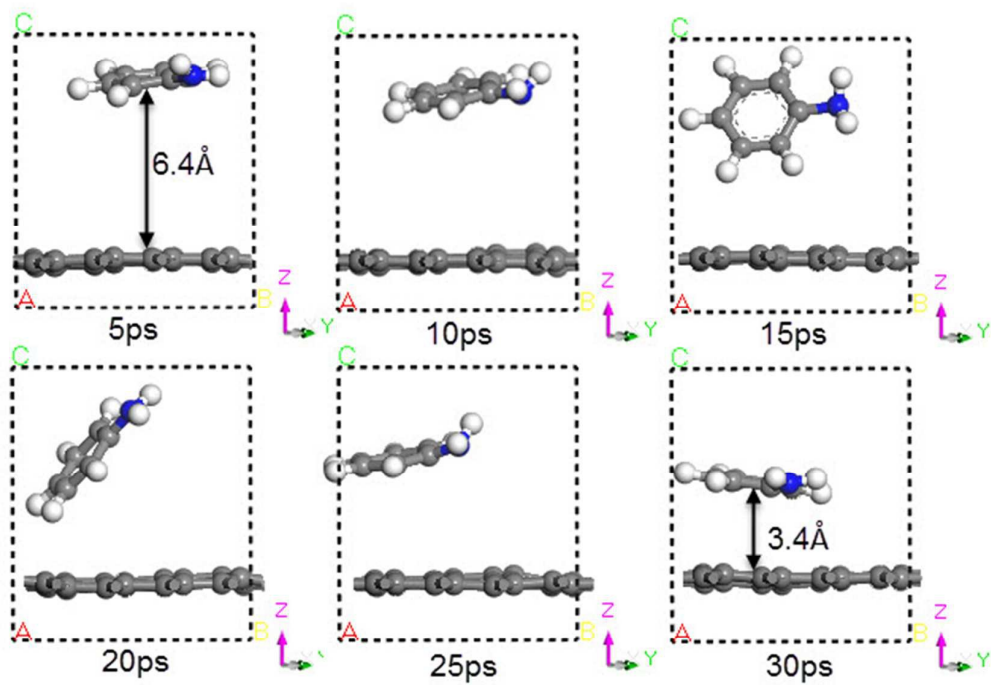
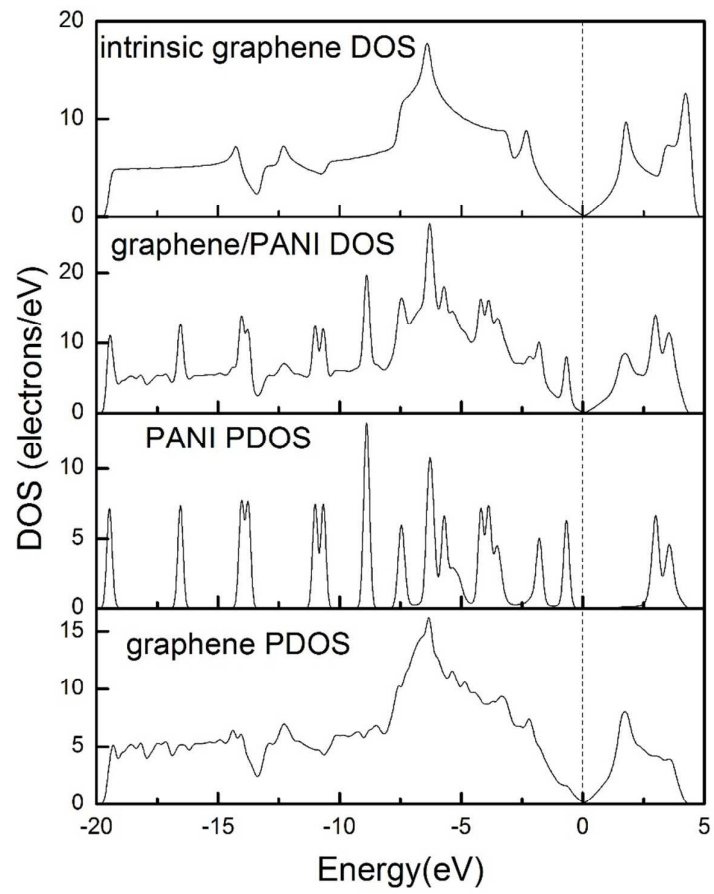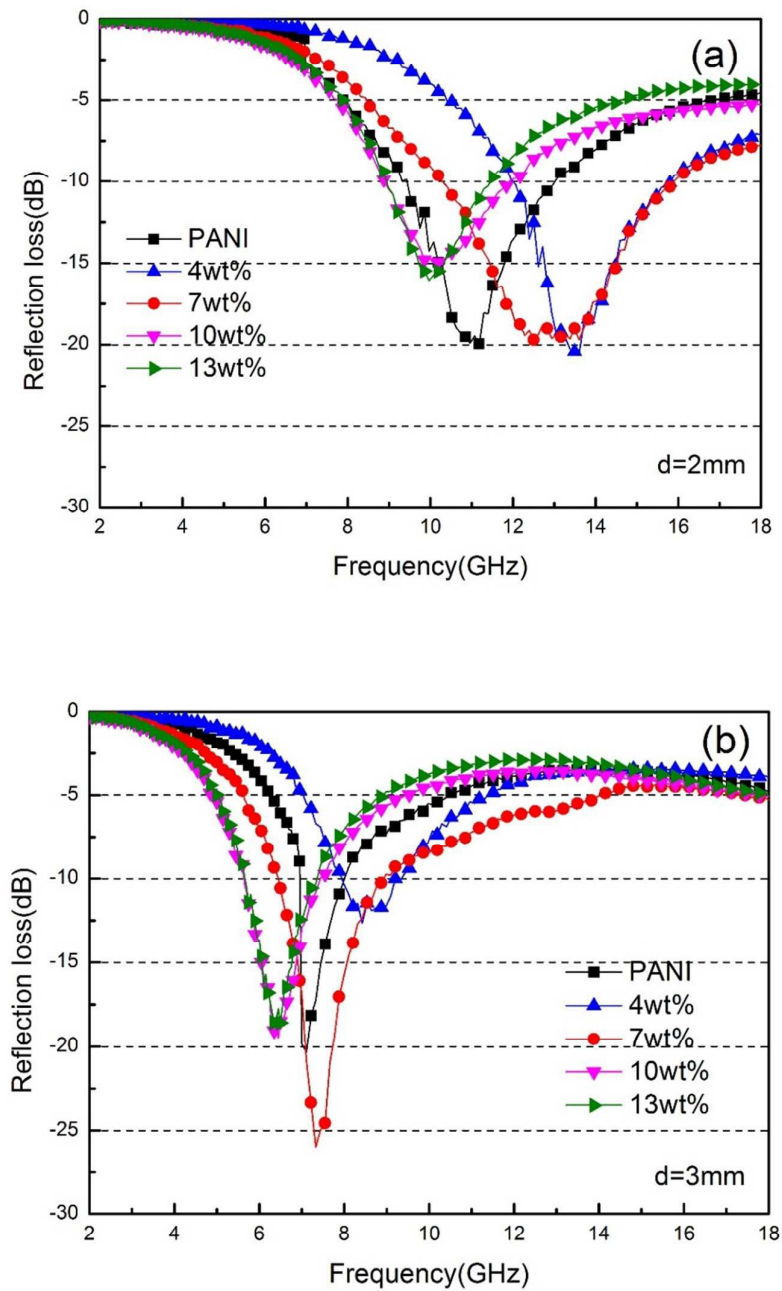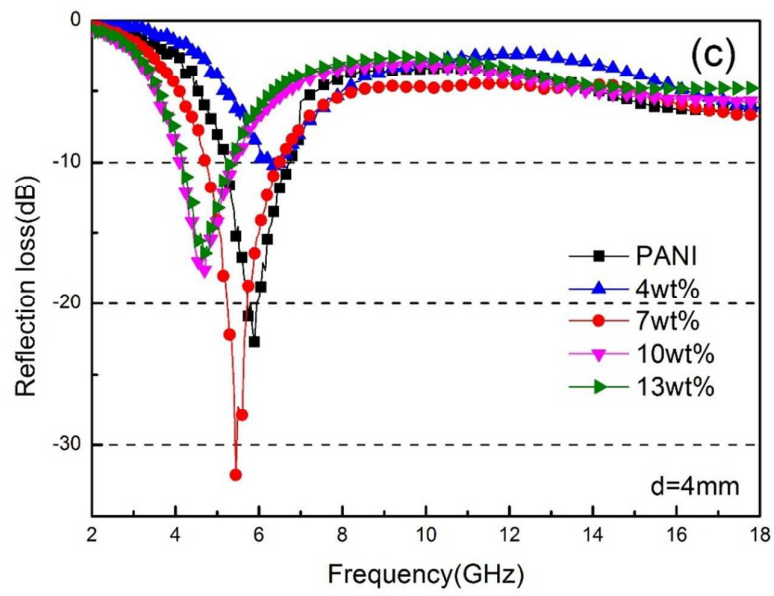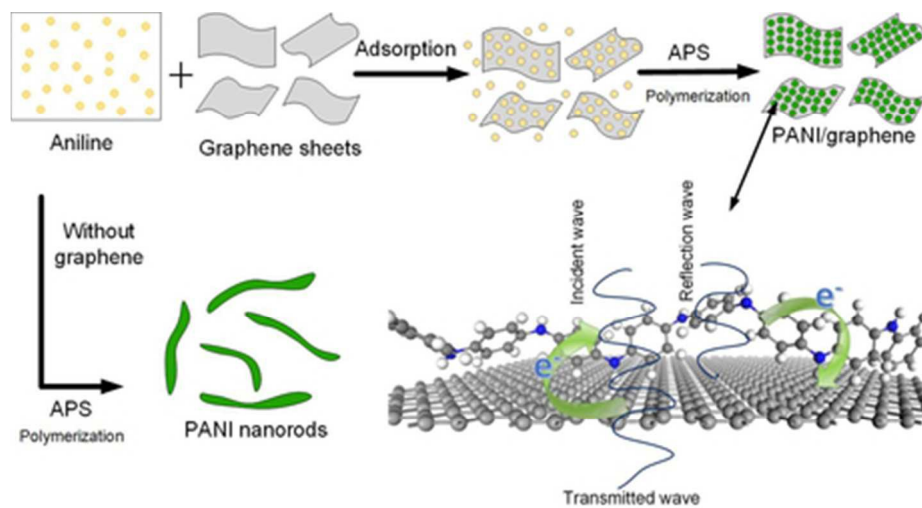Figure 10

Figure 11

The microwave dielectric properties of graphene-based polyaniline hybrids are studied based on experiments and first-principles calculation.

39x21mm (300 x 300 DPI)